Available online at www.sciencedirect.com

SCIENCE DIRECT®

Earth and Planetary Science Letters 225 (2004) 163–176

EPSL

www.elsevier.com/locate/epsl

Slip history of the Magnola fault (Apennines, Central Italy) from ^{36}Cl surface exposure dating: evidence for strong earthquakes over the Holocene

Luigi Palumbo[a,*], Lucilla Benedetti[b], Didier Bourlès[b], Aldo Cinque[a], Robert Finkel[c]

[a]*Dipartimento di Scienze della Terra, Università "Federico II" di Napoli, Largo S. Marcellino 10, 80138 Napoli, Italy*
[b]*CEREGE, UMR CNRS 6635, Université Aix-Marseille III, BP 80, plateau de l'Arbois, 13545 Aix en Provence, Cedex 04, France*
[c]*Lawrence Livermore National Laboratory–Center for Accelerator Mass Spectrometry, L-206, 7000 East Ave., Livermore, CA 94550, USA*

Received 30 March 2004; received in revised form 17 June 2004; accepted 18 June 2004

Editor: V. Courtillot

Abstract

To better understand the mechanics of deformation in the Mediterranean and the role that the convergence between Africa and Europe plays, it is necessary to know the deformation field at different time scales. Here we use in situ ^{36}Cl surface exposure dating of exposed bedrock fault scarps to determine earthquake time-slip histories and to quantify slip rates over the last several thousand years. This information allows us to delineate the seismic history of normal faulting within the Mediterranean area over that time period.

We have studied the limestone scarp produced by the Magnola fault in the Central Apennines, Italy. The Magnola fault, in the Fucino area, is an active, 15-km long, normal fault striking WNW and dipping SSW. The range front morphology, characterised by steep triangular facets separated by V-shaped valleys and wine-glass canyons, suggests that the Magnola fault has been active for at least the last several hundred thousand years. At the base of the facets, the fault cuts limestone bedrock to produce a well-preserved normal fault scarp 10 to 12 m high.

The distribution of ^{36}Cl concentration versus the height along that scarp is best explained by a minimum of five and a maximum of seven successive earthquake exhumations, with slips varying between 1.5 and 3 m. An age of ~5 ka at the base of the scarp and of ~12 ka at the top yields a slip rate of ~0.8 mm/year. The absence of any event on this fault during the last 5000 years suggests either that a future event is imminent on the Magnola fault or that the fault has entered a quiescent period with

* Corresponding author. Present address: CEREGE, UMR CNRS 6635, Université Aix-Marseille III, BP 80, plateau de l'Arbois, 13545 Aix en Provence, Cedex 04, France.

E-mail addresses: palumbo@cerege.fr (L. Palumbo), benedetti@cerege.fr (L. Benedetti), bourles@cerege.fr (D. Bourlès), cinque@unina.it (A. Cinque), rfinkel@llnl.gov (R. Finkel).

0012-821X/$ - see front matter
doi:10.1016/j.epsl.2004.06.012

much longer recurrence time. Our study confirms that the Magnola fault scarp is post-glacial and supports the hypothesis that similar scarps in the Mediterranean are also post-glacial.

Keywords: Apennines; seismotectonic; paleoseismology; Italy; cosmogenic dating; chlorine 36

1. Introduction

It is difficult to decipher the earthquake histories and displacement rates of faults whose only record of activity lies in bedrock scarps. However, chlorine 36 surface exposure dating of limestone scarps has recently been successfully applied to recover the seismic history of normal faults in Greece and in the Levant area [1–3].

The active tectonics of the Apennine chain is dominated by extension as suggested by focal mechanisms [4], (Fig. 1). The central and southern Apennines are the sites of the most significant historical and instrumental seismicity in western Europe (Benevento earthquake in 1456, $M \approx 7$, Neapolitan earthquake in 1857, $M \approx 7$, Avezzano earthquake in 1915, $M \approx 7$, Irpinia earthquake in 1980, M_s=6.9), [5,6]. Based on combined analysis of satellite images,

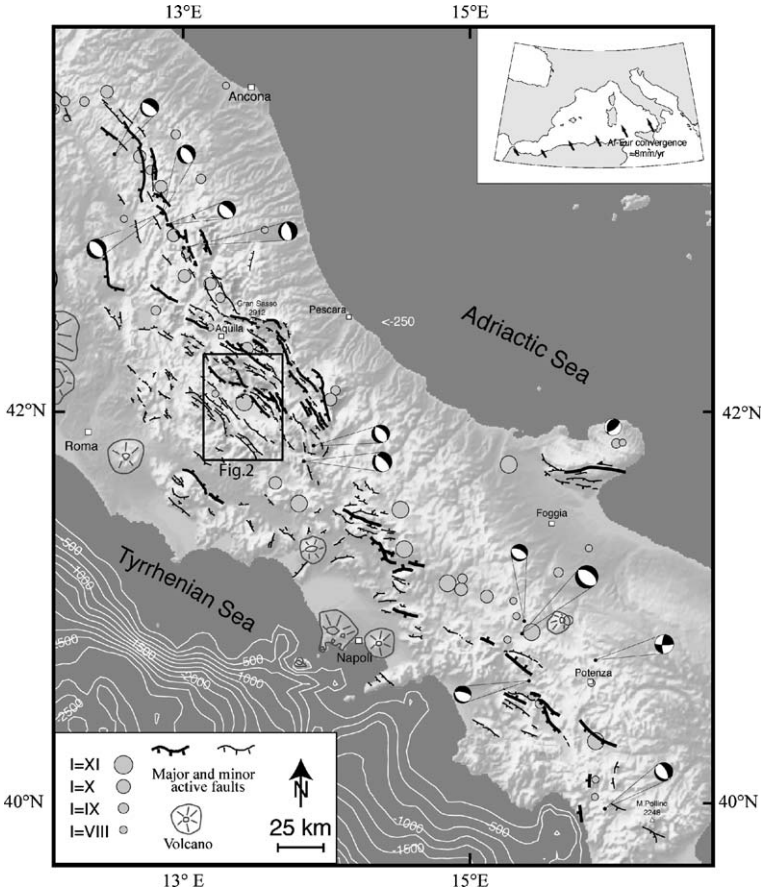

Fig. 1. Seismotectonic map of central and southern Apennines, modified from Benedetti [13]. Grey circles indicate location of historical earthquakes [5,6]; fault plane solutions are CMT solutions from Harvard (http://www.seismology.harvard.edu/data/).

topographical and geological maps and field observations, the active faults of this region have been mapped (Fig. 1), their most recent activity being commonly expressed by well-preserved limestone scarps [7–10]. However, most of the faults responsible for the major earthquakes are unknown and there is no long-term slip rate data in the Apennines.

Indeed, limestone scarps, while well adapted to chlorine 36 cosmogenic method, are ill-adapted to traditional trenching, rendering the techniques that have proved successful in other parts of the world, much less effective in Italy.

Recent deformation in Italy results from the convergence between Africa and Europe [11,12]. However, up to now, there is no kinematic model that integrates and explains the recent deformation of Italy, Africa's northernmost penetration into Europe in the plate tectonic framework [13]. Assessing long-term slip rates on the major active faults of Italy is essential in unraveling this problem. The approach we propose here will thus provide a way to recover paleoevents and to measure long-term slip rates on the active faults of Italy.

The Fucino, located in the central Apennines, is one of the most seismically active areas of Italy and was the epicentre of the catastrophic 1915 Avezzano earthquake ($I \approx XI$, $M_s \approx 7.0$) [5,6,14,15]. The area has been extensively studied by trenching (Table 1 and references therein). Reliable data on the seismic cycle of the area reach to about 5000 years before present and indicate recurrence times for strong events to be on the order of a thousand years. Up to now, no data exist for the longer-term earthquake history recorded in the bedrock scarps of the most prominent faults around the Fucino.

The Magnola fault, one of the main faults of the Fucino area, is capable of generating earthquakes up to magnitude 6.5 [7,9,16,17]. This fault is an approximately 15-km long active normal fault, striking WNW and dipping SSW in the Fucino area, about 80 km east of Rome (Fig. 2), whose most recent activity is expressed by a continuous limestone fault scarp. Using in situ produced cosmogenic ^{36}Cl, we have directly determined the continuous time-slip history for the last ~12,000 years. After a brief description of the morphology of the Magnola–Velino fault system, we then present the ^{36}Cl results collected

Table 1
Synthesis of paleoseismological data for the most prominent faults in the Fucino area based on (1) Giraudi [34], (2) Giraudi [35], (3) Giraudi [36], (4) Pantosti et al. [37], (5) Galadini and Galli [33], (6) Michetti et al. [38] and (7) this study. Star is for the 1915 event.

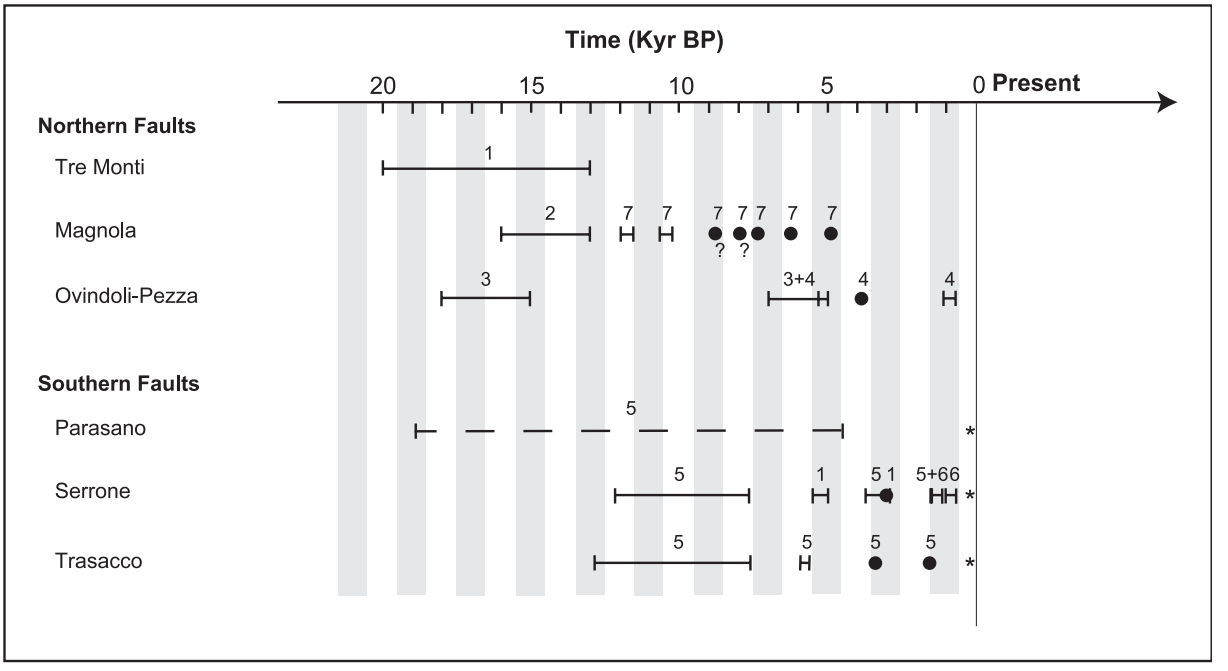

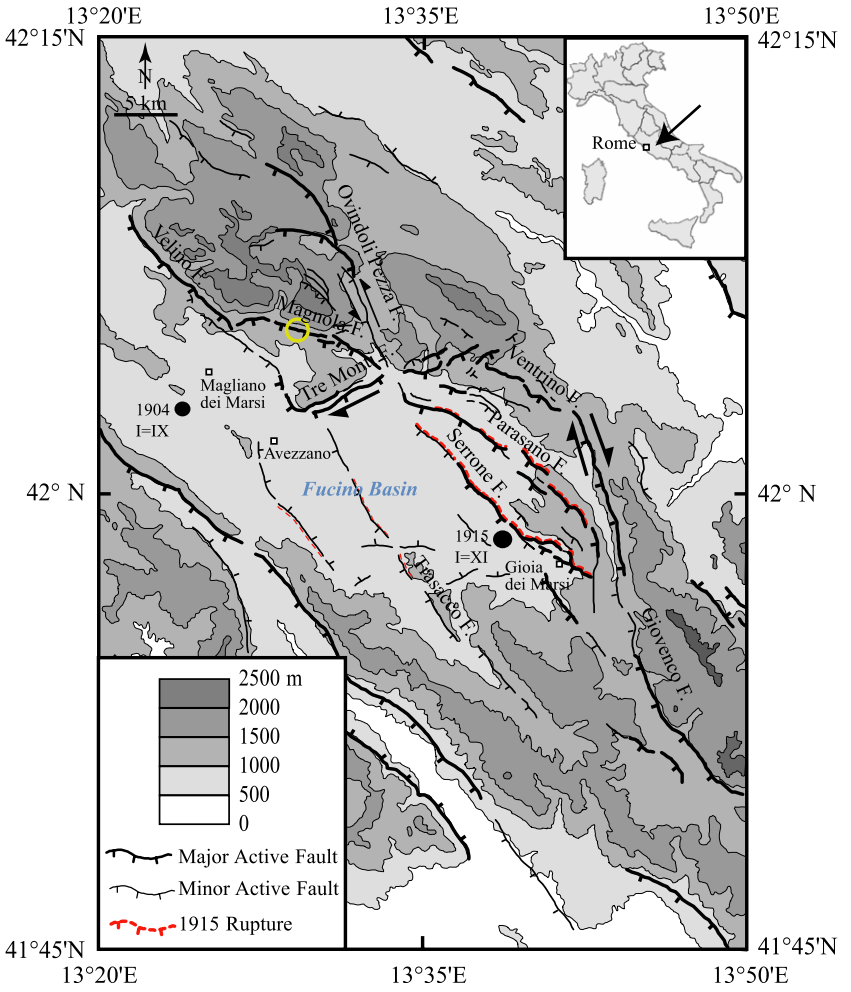

Fig. 2. Seismotectonic map of the Fucino area, modified from Piccardi et al. [9]. Circles mark locations of the studied site. The 1915 epicentre location is from [15] and from Monachesi and Stucchi [5] for the 1904 event. The 1915 surface ruptures are from Oddone [31] and Galadini and Galli [33].

at one site on the fault and the processes by which ^{36}Cl accumulates on the scarp. The numerical model used to interpret those data is described and our deduction of the most likely seismic history of the Magnola fault is discussed and confronted to the results obtained from previous studies on the paleoseismicity of the Fucino area.

2. The Magnola fault

The Apennine chain was formed during the Mio–Pliocene as the result of the subduction of the Adriatic under the opening Tyrrhenian Sea [11,12,18,19]. The associated thrust belt with NE shortening and NE verging built up the Central Apennines [18,20] (Fig. 1). It is not yet clear as to when or how the transition from Mio–Pliocene compression to present-day extension occurred. The timing of initiation of extension in the Apennines is still a matter of debate, with ages varying from early Quaternary to mid-Pleistocene [18,21,22].

The Apennines culminate at Gran Sasso with a maximum altitude of 2912 m a.s.l. Lying within mountains which culminate above 2000 m, the Fucino Basin is a very flat plain, about 30-km wide,

15-km long and with a mean elevation of about 650 m a.s.l. After deglaciation, the basin was flooded, forming a lake which was first drained by the Romans (≈50 AD) and then again in 1875 [23]. The basin is landlocked by active normal faults and appears roughly rhomb-shaped, with sides oriented NW–SE and ENE–WSW (Fig. 2).

North of the Fucino Basin, recent deformation is taken up by two major normal fault systems: the Magnola–Velino Fault and the Ovindoli–Pezza Fault (Fig. 2).

The Magnola and Velino faults, each about 15 km long, display the most spectacular topographic and geomorphic signatures of the faults that surround the

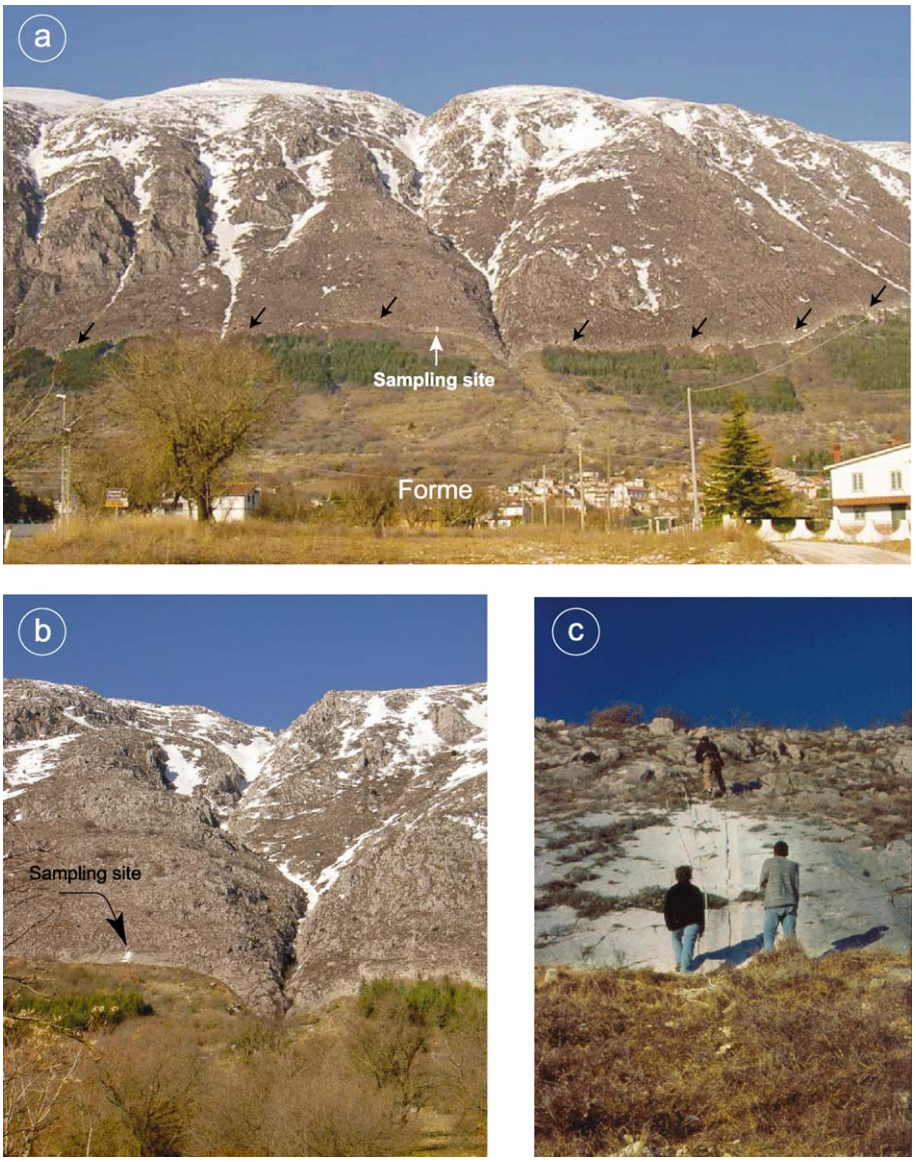

Fig. 3. Field views of the Magnola fault. (a) Picture of the Magnola fault. Arrows outlined the fault trace. The prominent triangular facets in this view are about 500-m high and note the perched valley just above the village named Forme. Note the regularity of scarp height and its continuity along the range front. (b) Close-up of cumulative scarp near Forme and sampling site. White mark is about 10-m high. (c) View of the sampling site. Samples are 20-cm wide, less than 2.5-cm deep and were divided into ~15 cm sections for measurement.

basin. They delimit the steep southwestern flank of the Magnola–Velino Mountains (2220–2468 m a.s.l., respectively), joining at an angle of 140° north of Magliano (Fig. 2).

The Magnola fault dips SSW and its trace runs for ≈15 km along the base of the SW slope of the Magnola mountain. There are two principal segments ≈10 and ≈5 km long, striking N110E and N130E, respectively. The two segments meet in a complex corner where faulting occurs along several parallel scarps on the hanging wall of the main fault escarpment (for a complete description of the fault, please refer to [9]).

Ongoing slip on this fault throughout the Quaternary is attested by the presence of triangular facets up to 500 m high with a slope greater than 30°, by the convex shape of mountain-front profiles and by wine-glass and perched valleys (Fig. 3a), [7,9,13,24,25]. At the base of the facets, a continuous cumulative scarp, with a steepness of about 50° with well-preserved dip-slip slicksensides present along its entire height, marks the contact between the Meso–Cenozoic carbonates and the colluvial deposits (Fig. 3) [9,16]. The maximum height of the scarp is 15–17 m, progressively decreasing towards the tips of the fault segments. There are few local variations on the scarp height due to differential erosion from active streams that cause the scarp to be locally higher (Fig. 3b). The regularity of the scarp (Fig. 3a) is powerful evidence that the scarp surface is due to fault slip alone and that there was no significant erosion or deposition on the hanging wall (except near active gullies) because the scarp began to form.

From detailed topographic profiles of the scarp, Piccardi et al. [9] infer a 3-m high maximum slip for the last event on this fault. They therefore deduced that the Magnola fault ruptured at least five times with an earthquake of magnitude up to M_w=6.7–7.0 during the Holocene and with recurrence times of 3000 to 1000 years. The throw rate they obtained is on the order of 0.7±0.3 mm/year.

3. ^{36}Cl production on the Magnola fault

We have used ^{36}Cl cosmic ray exposure dating to assess the earthquake slip history of the Magnola fault by determining exposure ages as a function of height on the cumulative scarp [cf. 1–3].

^{36}Cl is produced primarily through interactions of cosmic ray secondary neutrons and muons with Ca within the scarp limestone ($CaCO_3$), [26]. The production rate decreases exponentially with depth and ^{36}Cl thus mostly accumulates near the surface (Fig. 4). At sea level and high latitude, the ^{36}Cl production rate from Ca by fast neutrons is 48.8±3.4 atom/gCa/year and by muons is 2.1±0.4 atom/gCa/year [26,27].

In the central part of the fault, near the village of Forme, a continuous 20-cm-wide and about 2.5-cm-thick sample was collected along the limestone fault scarp. The particularly well-preserved scarp surface sampled was chosen far away from the river in order to avoid erosion and scarp exhumation due to river incision (Fig. 3b). It is therefore assumed that no significant erosion has affected the scarp. This assumption is supported by the morphological observations discussed above that are consistent with no significant erosion or deposition on the hanging wall.

The scarp was about 10-m high at the sampling site and was divided into ~15 cm sections for analysis. After grinding, leaching and chemical extraction of chlorine by precipitation of silver chloride in the CEREGE preparation laboratory, the ^{36}Cl and chloride concentrations in the carbonate were determined for 65 subsamples by isotope dilution accelerator mass spectrometry at the Lawrence Livermore National Laboratory CAMS facility (Table 2 and Fig. 5). Blanks were two orders of magnitude lower than the samples and replicates agreed to better than 5%.

The measured height profile of ^{36}Cl along the scarp was compared to synthetic ^{36}Cl profiles in order to determine whether the measured profile is consistent with seismic exhumation (Fig. 4). The model used includes all sources of production (energetic neutrons, thermal neutrons from various sources including slowed down energetic neutrons, stopped muons, Bremsstrahlung and spontaneous fission of U/Th) and uses sea-level, high-latitude production rates from Stone et al. [27]. These production rates were then scaled to the sampling latitude and elevation using the factors of Lal [28] and normalized to eliminate the effects of shielding by local topography following Gosse and Phillips [29] and references therein.

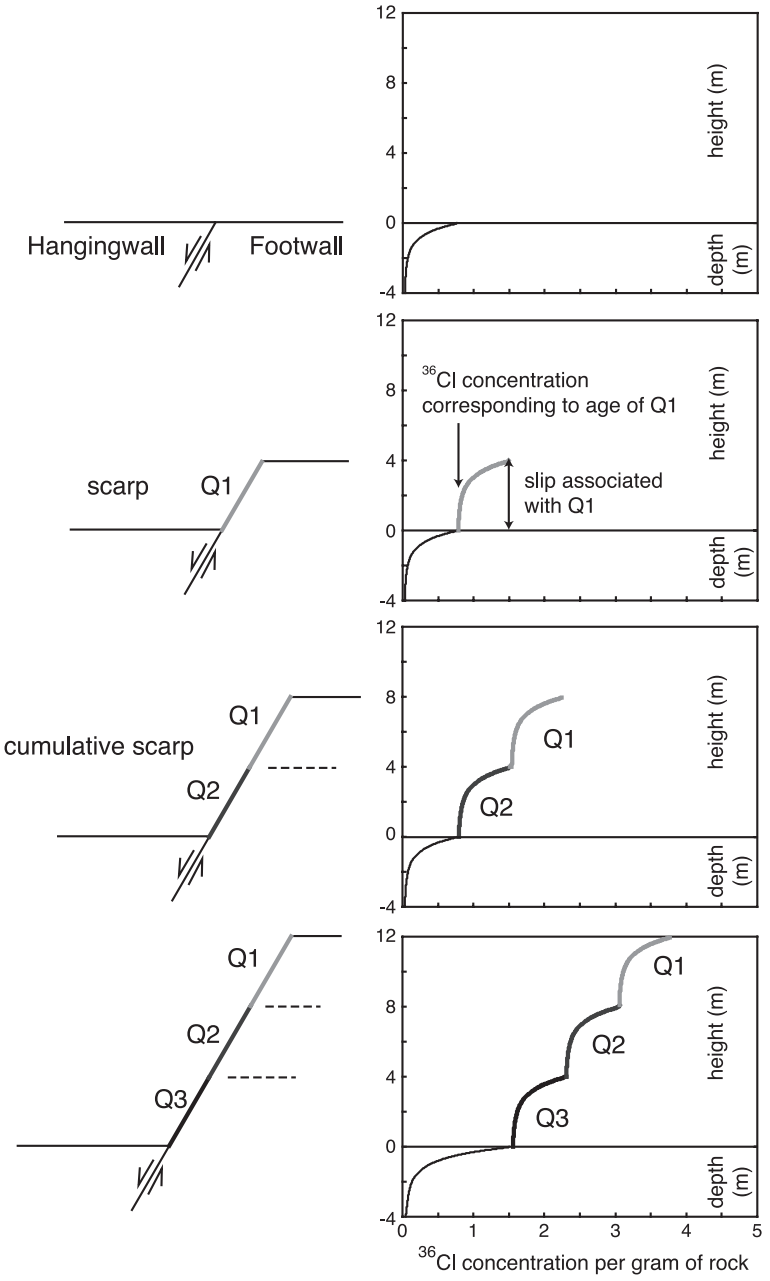

Fig. 4. Synthetic profiles for a scarp due to one (Q1), two (Q2) and three events (Q3), successively, with 4 m of slip each at 4000-year intervals. Because each earthquake uplifts a new portion of the scarp above the surface, the ^{36}Cl concentration along the scarp is the sum of ^{36}Cl accumulated before the earthquake below the surface and of ^{36}Cl accumulated after the earthquake above the surface. Modelling includes all sources of ^{36}Cl production from Stone et al. [26,27].

Fig. 4 shows synthetic profiles modelled for a scarp due to one, two and three successive events. Because each earthquake uplifts a new portion of the scarp above the surface, the ^{36}Cl concentration along the scarp is the sum of that ^{36}Cl produced below the surface prior to the earthquake and that

Table 2
^{36}Cl and chloride concentrations in the carbonate were determined by isotope dilution accelerator mass spectrometry at the LLNL CAMS facility

Sample name	Height (cm)	m_{rock} (g)	[Cl] ppm	$^{36}Cl/^{37}Cl$ in rock	±	^{36}Cl/g of rock	±
MAG 01	1010	23.54	16.3	7.2E−12	2.7E−13	4.81E+05	1.79E+04
MAG 02	1000	32.78	14.1	8.1E−12	3.0E−13	4.71E+05	1.74E+04
MAG 04	981	20.80	18.0	6.3E−12	2.2E−13	4.67E+05	1.19E+04
MAG 05	970	27.30	14.7	7.4E−12	2.3E−13	4.51E+05	1.39E+04
MAG 06	960	30.84	17.1	6.6E−12	2.0E−13	4.68E+05	1.45E+04
MAG 07	950	26.44	17.3	6.5E−12	2.4E−13	4.62E+05	1.70E+04
MAG 10	920	29.97	22.9	5.8E−12	2.7E−13	4.73E+05	1.78E+04
MAG 11	910	30.64	20.3	5.5E−12	2.0E−13	4.59E+05	1.64E+04
MAG 13	885	23.61	22.4	5.0E−12	1.3E−13	4.59E+05	1.25E+04
MAG 14	875	28.26	21.2	5.1E−12	1.9E−13	4.46E+05	1.64E+04
MAG 15	284	22.18	10.8	6.1E−12	2.9E−13	2.73E+05	1.29E+04
MAG 16	275	14.70	12.7	4.9E−12	1.2E−13	2.55E+05	4.99E+03
MAG 17	265	40.51	10.7	6.0E−12	2.0E−13	2.65E+05	8.68E+03
MAG 18	255	27.57	16.1	5.0E−12	2.3E−13	2.84E+05	1.07E+04
MAG 19	245	25.70	13.8	4.7E−12	1.8E−13	2.68E+05	9.96E+03
MAG 20	234	30.65	18.6	4.3E−12	1.9E−13	2.81E+05	1.01E+04
MAG 21	225	30.55	13.9	4.6E−12	1.7E−13	2.65E+05	9.89E+03
MAG 24	845	19.38	22.2	4.8E−12	1.3E−13	4.39E+05	9.59E+03
MAG 25	835	30.26	19.7	5.2E−12	1.7E−13	4.17E+05	1.38E+04
MAG 26	825	38.45	18.3	5.6E−12	2.1E−13	4.22E+05	1.58E+04
MAG 27	815	35.23	22.3	4.5E−12	1.7E−13	4.09E+05	1.58E+04
MAG 28	804	37.02	22.8	4.2E−12	1.0E−13	4.07E+05	8.39E+03
MAG 29	794	30.12	22.9	4.3E−12	1.6E−13	4.07E+05	1.52E+04
MAG 31	774	31.27	19.1	5.3E−12	2.3E−13	4.20E+05	1.79E+04
MAG 33	755	28.05	23.6	4.2E−12	2.1E−13	4.12E+05	2.02E+04
MAG 35	734	31.44	26.0	4.5E−12	2.1E−13	4.25E+05	1.61E+04
MAG 37	714	26.18	25.5	3.8E−12	1.4E−13	4.01E+05	1.49E+04
MAG 39	695	25.94	20.1	4.4E−12	1.1E−13	3.74E+05	7.89E+03
MAG 41	675	27.01	9.9	8.7E−12	2.6E−13	3.53E+05	1.09E+04
MAG 43	655	28.48	8.9	9.6E−12	4.1E−13	3.54E+05	1.52E+04
MAG 45	636	31.87	9.8	9.1E−12	4.5E−13	3.70E+05	1.81E+04
MAG 47	214	25.38	15.3	4.2E−12	2.0E−13	2.62E+05	1.24E+04
MAG 49	195	19.83	15.7	4.0E−12	1.8E−13	2.58E+05	1.15E+04
MAG 50	187	29.41	13.6	4.3E−12	1.6E−13	2.41E+05	8.92E+03
MAG 52	166	24.68	13.8	4.1E−12	9.2E−14	2.39E+05	3.94E+03
MAG 53	156	28.48	12.8	4.9E−12	1.5E−13	2.60E+05	7.97E+03
MAG 55	131	22.16	12.3	5.7E−12	2.7E−13	2.45E+05	9.26E+03
MAG 57	111	24.63	9.4	5.7E−12	3.5E−13	2.20E+05	1.35E+04
MAG 58	101	27.60	10.3	5.2E−12	2.9E−13	2.20E+05	1.24E+04
MAG 60	81	29.24	11.5	4.6E−12	2.7E−13	2.16E+05	1.28E+04
MAG 62	61	28.44	11.0	4.6E−12	1.6E−13	2.09E+05	7.48E+03
MAG 63	51	25.70	10.8	5.0E−12	2.0E−13	2.21E+05	8.66E+03
MAG 65	28	30.32	11.9	4.7E−12	1.5E−13	2.29E+05	7.54E+03
MAG 66	615	39.36	9.1	8.8E−12	3.8E−13	3.29E+05	1.42E+04
MAG 67	605	29.59	9.3	9.1E−12	3.4E−13	3.49E+05	1.30E+04
MAG 69	585	29.20	12.3	6.6E−12	2.5E−13	3.33E+05	1.25E+04
MAG 70	574	23.47	12.9	6.6E−12	2.4E−13	3.49E+05	1.29E+04
MAG 72	554	32.08	11.5	6.7E−12	3.5E−13	3.17E+05	1.65E+04
MAG 73	545	24.54	12.7	6.2E−12	1.5E−13	3.27E+05	6.44E+03
MAG 75	525	25.42	14.4	5.1E−12	2.3E−13	3.05E+05	1.38E+04
MAG 76	515	25.37	13.7	5.4E−12	1.6E−13	3.03E+05	9.37E+03

Table 2 (*continued*)

Sample name	Height (cm)	m_{rock} (g)	[Cl] ppm	$^{36}Cl/^{37}Cl$ in rock	±	^{36}Cl/g of rock	±
MAG 77	504	30.19	12.1	6.3E−12	2.3E−13	3.12E+05	1.14E+04
MAG 78	494	25.56	9.1	7.9E−12	2.9E−13	2.97E+05	1.11E+04
MAG 80	474	16.53	6.5	1.1E−11	3.3E−13	2.98E+05	6.81E+03
MAG 82	455	30.00	6.5	1.3E−11	5.9E−13	2.90E+05	1.10E+04
MAG 83	445	26.02	9.0	8.2E−12	2.8E−13	3.03E+05	1.03E+04
MAG 84	435	28.24	13.6	4.9E−12	1.9E−13	2.73E+05	1.07E+04
MAG 85	425	24.83	10.9	6.1E−12	1.7E−13	2.75E+05	5.47E+03
MAG 86	414	26.31	10.9	6.0E−12	3.9E−13	2.76E+05	1.47E+04
MAG 88	394	31.43	16.2	4.2E−12	1.2E−13	2.81E+05	6.00E+03
MAG 89	387	29.66	16.7	4.0E−12	1.5E−13	2.75E+05	1.02E+04
MAG 90	383	35.59	12.6	5.5E−12	2.1E−13	2.84E+05	1.06E+04
MAG 91	373	29.14	15.3	5.2E−12	2.4E−13	2.79E+05	1.06E+04
MAG 92	363	29.11	15.1	4.5E−12	1.7E−13	2.78E+05	1.04E+04
MAG 93	353	29.47	15.5	4.4E−12	1.3E−13	2.83E+05	6.84E+03

Calcium content was measured every 40 cm along the scarp by ICP at CEREGE, with an average of 36% of calcium in each samples. Stone et al. [26,27] production rate derived from Ca-rich mineral was used. ^{36}Cl measurements were standardized relative to NIST ^{36}Cl standard. Replicates were within 5% and blanks were two orders lower than the samples.

accumulated above the surface after the earthquake (Fig. 4). The model is therefore iterative, with the number of events, their timing and the magnitude of the associated slip strongly influencing the shape of the whole profile. This is clearly depicted in Fig. 4. For a scarp being seismically exhumed, the characteristic profile is therefore a series of exponentials with discontinuities marking the earthquakes.

Various scarp emplacement scenarios were tested. They include scarp formed by steady creep (model with several small events with slip of less than 10 cm per event), by differential erosion (model with a continuous movement of various height at various period of time), by a unique event (equivalent to a scenario of gravitational collapse) and by seismic events (model with instantaneous events at various periods of time and with varying slip). For each scenario, the best fit was determined by calculating the root-mean-square between the data and the model [30], with n as the number of data points:

$$\mathrm{RMS} = \sqrt{\sum_{n} \left({}^{36}\mathrm{Cl}_{\mathrm{measured}} - {}^{36}\mathrm{Cl}_{\mathrm{model}} \right)^2 / n}$$

Then the "best" scenario was determined by calculating for each "best" model scenario the Aikake Information Criterion (Fig. 5b). This criterion includes not only the "goodness-of-fit" between the model and the data, but also the number of parameters included in the model [30], with n the number of data points and p the number of independent parameters which corresponds to the number of events:

$$\mathrm{AIC} = n\log\left[\sum_{n} \left({}^{36}\mathrm{Cl}_{\mathrm{measured}} - {}^{36}\mathrm{Cl}_{\mathrm{model}} \right)^2 / n \right] + 2p$$

4. Seismic history of the Magnola fault

The results obtained on the sampled scarp show that the Magnola fault scarp was not formed by steady creep, differential erosion or gravitational collapse, but rather by at least four earthquakes (Fig. 5b). In agreement with the experimental profile where four discontinuities, two at the top and two at bottom, are prominent, displacement scenarios considering less than four events or more than eight are clearly less consistent with the data (Fig. 5b). The scenario with six earthquakes yield the best AIC value, but models with seven or five events do not have significantly higher AIC value (Fig. 5b). All three models yield similar displacement scenarios for the bottom and top parts of the scarp, while in the central part of the profile, modelling is less straightforward (Fig. 5c). Five events at 4.8, 6.7, 7.4, 10.5 and 12.0 ka with slips varying from 275 to 155 cm are well constrained by the modelling.

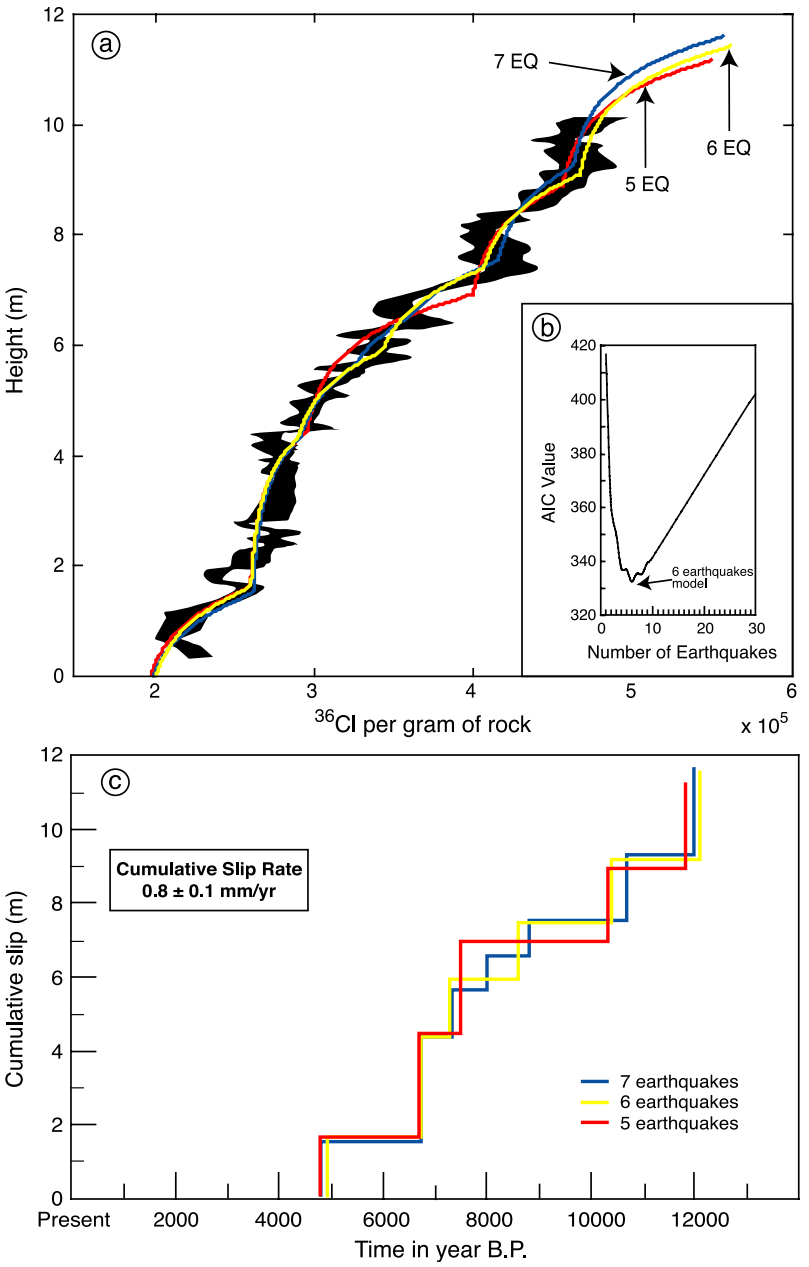

Fig. 5. (a) The black curve represents the envelop of the ^{36}Cl concentration per gram of rock versus the height of the scarp including error bars (less than 7% for each sample). See Table 2 for details on the data points of the curve. The colour lines (see online version of this article) represent the three models best fitting the data with 5, 6 and 7 earthquakes. (b) AIC versus the number of earthquakes for each best model scenario. Note that AIC values are high with 1 event or with more than 10. AIC is minimised for displacement scenario with more than four events and with less than eight. (c) Seismic history of the Magnola fault. Cumulative slip versus the age of seismic events for the three best models. Note that the first two events and the last two events are well constrained. ^{36}Cl synthetic profiles were calculated with a ^{36}Cl decay constant of 2.303 10^{-6} year^{-1}, shielding factor is 0.72 [29]. At sea level and high latitude, the ^{36}Cl production rate by fast neutrons is 48.8±3.4 atom/gCa/year and by muons 2.1±0.4 atom/gCa/year [26,27]. Correction factors for the production rate at our site latitude (42.12°) and altitude (1252 m) were 2.75 and 1.71 for neutrons and muons, respectively [28].

Two additional events at 8 and 8.8 ka, with slips of 90 and 100 cm, respectively, are inferred but remain hypothetical (Fig. 5c). The age of the last earthquake with an associated slip of 155±15 cm on the Magnola fault scarp is thus 4850±450 ka, while from the oldest to the most recent, intervals of 1500, 3100, 700 and 1900 years separate the five earthquakes of the proposed sequence.

5. Paleoseismicity of the Fucino area

On January 15, 1915, an earthquake, I≈XI MCS, $M_s \approx 7.0$, destroyed most of the villages around the Fucino Plain, causing more than 30,000 victims (Fig. 2) [14]. The surface faulting, striking NW–SE, along the Serrone and Parasano faults on the east side of the Fucino Basin, was mapped by several authors with a maximum vertical throw of 3 m (Fig. 2) [31,32]. The Trasacco fault is also supposed to have ruptured during this event [33]. Only 11 years before, in 1904, an event of intensity IX struck the northern Fucino area, damaging several villages on the slopes of Mt. Velino [5,14]. No surface rupture was reported and the fault responsible for this event is unknown.

Palaeoseismological studies infer the occurrence of other earthquakes similar to that of 1915 in the Fucino Basin during the Late Pleistocene and Holocene (Table 1).

Based on dating of glacial deposits that have been offset by normal faults, Giraudi [34] infers that the Tre-Monti fault (Fig. 2) ruptured during an event that might have occurred between 20 and 13 years B.P. (Table 1).

On the northeastern slope of Mt. Magnola (Fig. 2), Giraudi [35] mapped small scarps (≈1-km long each) striking WNW–ESE, reaching 6-m high, offsetting moraine deposits he assigned to a period of glacial retreat between 16 and 13 kyr B.P. (Table 1).

Lastly, on the E–W segment of the Ovindoli–Pezza fault system, which strikes parallel to Mt. Magnola scarps and runs a few km north (Fig. 2), Giraudi [36] suggests that two distinct events occurred, the first one between 18 and 15 kyr B.P., and the second between 7 and 5 kyr B.P. (Table 1). From detailed geomorphological study and logging of several trenches dug across the Ovindoli–Pezza fault, Pantosti et al. [37] demonstrated the occurrence of three earthquakes on this fault over the Holocene. The first one occurred between 5000 and 3300 BC, the second about 1900 BC and the last one between 860 and 1300 AD, the slip per event ranging from 2 to 3 m high (Table 1). Based on those results and on geomorphic features, Pantosti et al. [37] calculate a long-term slip-rate of 0.7–1.2 mm/year. This implies a recurrence time on this fault of 1000 to 3000 years. Therefore, two independent studies [36,37], based on different types of observation, suggest that an important event occurred on the Ovindoli–Pezza fault between 7000 and 5000 years B.P. (Table 1).

Geomorphological and paleontological observations suggest that the Serrone fault (Fig. 2) was active around 5500–5000 years B.P. and about 3100 years ago, while fault scarps in the centre of the former lake suggest a late-Roman or Middle Ages (2000 years B.P. to 1000 years B.P.) seismic event [34]. Trench investigations showed evidence for two paleo-earthquakes on this same fault [38]: one constrained to have occurred between the 6th and 9th centuries AD and associated with the 801 AD historical event that struck Central Italy [5,6]; the second constrained between the 10th century AD and 1349 AD (Table 1). Other authors [33] infer that three events occurred on this fault, the first one between 10,231 and 5576 BC, the second between 1700 and 833 BC, and the one prior to 1915, between 426 and 782 AD. Therefore, these studies agree on one event, which might have occurred between the 6th and 9th centuries AD on the Serrone fault (Table 1).

Trench investigation across the Parasano fault (Fig. 2) produced evidence for three ruptures prior to 1915 during the last 19 kyr [33].

Based on hand-borehole observations and trench investigations, the same authors deduced that the Trasacco fault (Fig. 2) ruptured four times before 1915. The first event occurred between 10,729 and 5576 BC, the second in 3944–3618 BC, the third between the 16th and 15th centuries BC and the last one between the 5th and 6th centuries AD.

The studies presented above suggest that the Parasano, Serrone and Trasacco faults could have ruptured simultaneously as they did in 1915. Recurrence times on the Ovindoli–Pezza fault, in agreement with the one proposed by Piccardi et al. [9] on the Magnola fault, are between 3000 and 1000 years, much longer than that inferred on the southern faults.

6. Discussion and conclusions

The ^{36}Cl concentrations measured along the Magnola fault scarp indicate that slip has accumulated on this scarp over the last 12 kyr. This yields a cumulative slip rate of 0.8±0.1 mm/year, similar to that of 0.7±0.3 mm/year proposed for the same fault by Piccardi et al. [9] and to that of 0.7–1.2 mm/year proposed for the Ovindoli–Pezza fault by Pantosti et al. [37]. If constant over several thousand of years, this slip rate implies that the 500-m high triangular facets have been created in about a million years.

When compared to modelled synthetic ^{36}Cl profiles, the experimental ^{36}Cl profile obtained on the Magnola fault yields recurrence times between 3000 to 1000 years, in agreement with those deduced from various trenching and geomorphological studies done on faults north of the Fucino [9,34,35,37].

The experimental ^{36}Cl profile also shows that the last event on the Magnola fault occurred at 4850±450 ka, with a slip of 155±15 cm. This is in agreement with geomorphological observations completed by detailed topographic profiles suggesting that the last event on this fault occurred about 5000 years ago, with a slip between 3 and 1 m [9]. If the whole 15-km-long fault ruptured, the magnitude of the event would have been ~6.7 [39]. However, the slip amplitudes of all four previous events range from 200 to 280 cm. Considering scaling laws [39,40], events this large should have simultaneously ruptured the northern Velino segment and thus produce seismic events with a magnitude close to 7, similar to that of the 1915 earthquake.

Pantosti et al. [37] suggested that two events, one between 5300 and 7000 and the other ~3900 years B.P. ago, occurred on the Ovindoli–Pezza fault with a slip per event ranging from 2 to 3 m (Fig. 2 and Table 1). The E–W segments of the Ovindoli–Pezza fault are located a few kilometres north of the Magnola fault and strike parallel to it (Fig. 2). The ages of the earthquakes inferred by Pantosti et al. [37] on those segments are close to the ages of the penultimate and ultimate events we deduced on the Magnola fault (Table 1). The geometry of those faults suggests that they should connect at depth. Therefore, in terms of their seismic behaviour, this might imply that either they could have ruptured simultaneously, as the Parasano and Serrone faults did in 1915, or that an event on one could have triggered another event on the second fault. Dating the limestone fault scarp on the Ovindoli–Pezza fault would allow to farther evaluating the relationships of those two faults in the past through comparison of their seismic behaviour during the last 12 kyr. This is important because the last event recorded on the Ovindoli–Pezza fault by Pantosti et al. [37] occurred 1200 to 700 years ago. On the other hand, our results show that the last event on the Magnola fault occurred ~4850 years ago, twice the average recurrence time deduced for the previous four events. This might suggest either that a future event is imminent on the Magnola fault or that the fault has entered a more quiescent period with much longer recurrence time. This latter could be due to a change in the loading rate on the Magnola fault because of stress interactions with the surrounding faults, for example, the Ovindoli–Pezza, as previously inferred in other regions [2,41].

This study confirms that the Magnola fault scarp is post-glacial and adds support to the hypothesis that all such similar scarps in the Mediterranean are post-glacial [2,9,42]. Indeed, several authors have suggested that similar fault scarps in the Mediterranean are post-glacial in age [2,9,16,42]. In Greece, a recent ^{36}Cl study has also quantitatively confirmed this hypothesis, with a maximum age for such limestone fault scarps of about 12 ka [2]. During the last glacial maximum, the prevailing dry, cold climate [43,44] inhibited the formation of vegetation cover on the mountain slopes, thus exposing newly formed scarps to burial by periglacial superficial mass transport. After deglaciation, vegetation reoccupied the mountain slopes due to the prevailing wet, warm climate. Consequently, superficial mass transport was interrupted and increments of throw along the fault trace were no longer buried. These changed conditions allowed the preservation of post-glacial scarps and the steady growth of the cumulative scarp as the result of successive earthquakes [2,42].

This result opens new possibilities of calculating Holocene deformation rate in Italy, which has been impossible up to now. When compared with the data from the dense GPS networks in the region [45], this will provide a unique view of the deformation field at different time scales, important to understand the mechanics of deformation in the Mediterranean and the relationships with the Africa–Europe convergence.

Acknowledgments

We are grateful to Philippe Chamaret and Fabio Villani for helping us in field work. Alessandro Ercole and Corpo Forestale are greatly acknowledged for authorizing us to work in the Velino Park. This work benefited from fruitful discussions with Alessandra Ascione, Régis Braucher, Olivier Bellier and Bruno Hamelin. We acknowledge the two referees for their thorough reviews that improved the manuscript. This work was supported by the Fondi Vinci from the Italian–French University, prot. UFI2I4CH7T. Dating was performed under the auspices of U.S. Department of Energy by the University of California, Lawrence Livermore National Laboratory under Contract No. W-7405-Eng-48.

References

[1] S. Gran Mitchell, A. Matmon, P.R. Bierman, M. Caffee, D. Rizzo, Displacement history of a limestone normal fault scarp, northern Israel, from cosmogenic ^{36}Cl, J. Geophys. Res. 106 (2001) 4247–4264.

[2] L. Benedetti, R. Finkel, D. Papanastassiou, G. King, R. Armijo, F.J. Ryerson, D. Farber, F. Flerit, Post-glacial slip history of the Sparta fault (Greece) determined by 36Cl cosmogenic dating: evidence for non-periodic earthquakes, Geophys. Res. Lett. 27 (2002) doi:10.1029/2001GL014510.

[3] L. Benedetti, R. Finkel, G. King, R. Armijo, D. Papanastassiou, F.J. Ryerson, F. Flerit, D. Farber, G. Stvrakakis, Motion on the Kaparelli fault (Greece) prior to the 1981 earthquake sequence determined from ^{36}Cl cosmogenic dating, Terra Nova 15 (2003) 118–124.

[4] A. Frepoli, A. Amato, Contemporaneous extension and compression in the Northern Apennines from earthquakes fault-plane solutions, Geophys. J. Int. 129 (1997) 368–388.

[5] G. Monachesi, M. Stucchi, DOM4.1, un database di osservazioni macrosismiche di terremoti di area italiana al di sopra della soglia di danno, GNDT, Milan, available on the world wide web at http://emidius.itim.mi.cnr.it/DOM/home.html, 1997.

[6] E. Boschi, G. Ferrari, P. Gasperini, E. Guidoboni, G. Smriglio, G. Valensise, Catalogo dei Forti Terremoti in Italia dal 461 a.C. al 1980, ING e SGA, 1995, 973 pp.

[7] C. Bosi, Osservazioni preliminari su faglie probabilmente attive nell'Appennino centrale, Boll. Soc. Geol. Ital. 94 (1975) 827–859.

[8] A.M. Blumetti, F. Dramis, A.M. Michetti, Fault-generated mountain in the Central Apennines (Central Italy): geomorphological features and seismotectonics implications, Earth Surface Landf. 18 (1993) 203–223.

[9] L. Piccardi, Y. Gaudemer, P. Tapponier, M. Boccaletti, Active oblique extension in the central Apennines (Italy): evidence from the Fucino region, Geophys. J. Int. 139 (1999) 499–530.

[10] C. Giraudi, Consideration on the significance of some post-glacial fault scarps in the Abruzzo Apennines (Central Italy), Quat. Int. 25 (1995) 33–45.

[11] D.P. McKenzie, Active tectonics of the Mediterranean region, Geophys. J. R. Astron. Soc. 30 (1972) 109–185.

[12] P. Tapponnier, Évolution tectonique du système alpin en Méditerranée: poinçonnement et écrasement rigide-plastique, Bull. Soc. Geol. Fr. 7 (1977) 437–460.

[13] L. Benedetti, Sismotectonique de l'Italie et des régions adjacentes: fragmentation du promontoire adriatique, Thèse de Doctorat de l'Université Paris VII, 1999, p. 358.

[14] C. Margottini, S. Screpanti, Attribuzione della magnitudo al terremoto di Avezzano del 13 gennaio 1915 e studio dell'evoluzione temporale della crisi sismica associata, in: S. Castanetto, F. Galadini (Eds.), 13 gennaio 1915—il terremoto della Marsica, Servizio Sismico Nazionale, CNR-IRTR, Roma, 1999, pp. 301–318.

[15] D. Molin, F. Galadini, P. Galli, L. Mucci, A. Rossi, Terremoto del Fucino del 13 gennaio 1915. Studio Macrosismico, in: S. Castanetto, F. Galadini (Eds.), 13 gennaio 1915—il terremoto della Marsica, Servizio Sismico Nazionale, CNR-IRTR, Roma, 1999, pp. 321–340.

[16] G.P. Roberts, A.M. Michetti, Spatial and temporal variations in growth rates along active normal fault systems: an example from The Lazio–Abruzzo Apennines, central Italy, J. Struct. Geol. 26 (2004) 339–376.

[17] N.C. Morewood, G.P. Roberts, The geometry, kinematics and rates of deformation within an en échelon normal fault segment boundary, central Italy, J. Struct. Geol. 22 (2000) 1027–1047.

[18] A. Malinverno, W.B.F. Ryan, Extension in the Tyrrhenian sea and shortening in the Apennines as result of arc migration driven by sinking of the lithosphere, Tectonics 5 (1986) 227–245.

[19] E. Patacca, P. Scandone, Post-Tortonian mountain building in the Apennines: the role of the passive sinking of a relic lithospheric slab, in: A. Boriani, et al. (Eds.), The Lithosphere in Italy, Academia Nazionale dei Lincei, Roma, 1989, pp. 157–176.

[20] E. Patacca, R. Sartori, P. Scandone, Tyrrhenian Basin and Apenninic arcs: kinematic relations since Late Tortonian times, Mem. Soc. Geol. Ital. 45 (1990) 425–451.

[21] A. Cinque, E. Patacca, P. Scandone, M. Tozzi, Quaternary kinematic evolution of the Southern Apennines. Relationship between surface geological features and deep lithospheric structures, Ann. Geofis. 36 (1993) 443–460.

[22] J.C. Hippolyte, J. Angelier, F. Roure, A major geodynamic change revealed by Quaternary stress patterns in the Southern Apennines (Italy), Tectonophysics 230 (1994) 199–210.

[23] C. Giraudi, Lake levels and climate for the last 30000 years in the Fucino area (Abruzzo, Central Italy): a review, Palaeogeogr. Palaeoclimatol. Palaeoecol. 70 (1989) 249–260.

[24] C. Giraudi, Faglie ad attività olocenica nella Piana del Fucino (Abbruzzo), Mem. Soc. Geol. Ital. 35 (1986) 875–880.

[25] C. Giraudi, Considerations on the significance of some post-glacial fault scarps in the Abruzzo Apennines (central Italy), Quat. Int. 25 (1995) 33–45.

[26] J.O.H. Stone, L.K. Fifield, G.L. Allan, R.G. Cresswell, Cosmogenic chlorine-36 from calcium spallation, Geochim. Cosmochim. Acta 60 (1996) 679–692.
[27] J.O.H. Stone, J.M. Evans, L.K. Fifield, G.L. Allan, R.G. Cresswell, Cosmogenic chlorine-36 production in calcite by muons, Geochim. Cosmochim. Acta 62 (1998) 433–454.
[28] D. Lal, Cosmic ray labelling of erosion surfaces: in situ nuclide production rates and erosion model, Earth Planet. Sci. Lett. 104 (1991) 424–439.
[29] J.C. Gosse, F.M. Phillips, Terrestrial in situ cosmogenic nuclides: theory and application, Quat. Sci. Rev. 20 (2001) 1475–1560.
[30] J.R. Taylor, An Introduction to Error Analysis, the Study of Uncertainties in Physical Measurements, 2nd ed., University Science Books, Sausalito, CA, 1997, 327 pp.
[31] E. Oddone, Gli elementi fisici del grande terremoto marsicano fucense del 13 gennaio 1915, Boll. Soc. Sismol. Ital. 19 (1915) 71–215.
[32] L. Serva, A.M. Blumetti, A.M. Michetti, Gli effetti sul terreno del terremoto del Fucino (13 Gennaio 1915); tentativo di interpretazione della evoluzione tettonica recente di alcune strutture, Mem. Soc. Geol. Ital. 35 (1986) 893–907.
[33] F. Galadini, P. Galli, The Holocene paleoearthquakes on the 1915 Avezzano earthquake faults (central Italy): implications for active tectonics in the central Apennines, Tectonophysics 308 (1999) 143–170.
[34] C. Giraudi, Evoluzione geologica della piana del Fucino (Abruzzo) negli ultimi 30000 anni, Quaternario 1 (1988) 131–159.
[35] C. Giraudi, Segnalazione di scarpate di faglia tardo-pleistoceniche sui monti della Magnola (Massiccio del Velino–Abruzzo), Quaternario 5 (1992) 27–32.
[36] C. Giraudi, Datazione con metodi geologici delle scarpate di faglia post-glaciali di Ovindoli–Piano di Pezza (Abruzzo–Italia Centrale): implicazioni, Mem. Soc. Geol. Ital. 42 (1989) 29–39.
[37] D. Pantosti, G. D'Adezzio, F.R. Cinti, Paleoseismicity of the Ovindoli–Pezza fault, central Apennines, Italy: a history including a large, previously unrecorded earthquake in the Middle Ages (860–1300 A.D.), J. Geophys. Res. 101 (1996) 5937–5959.
[38] A.M. Michetti, F. Brunamonte, L. Serva, E. Vittori, Trench investigations of the 1915 Fucino Earthquakes, J. Geophys. Res. 101 (1996) 5921–5936.
[39] C.H. Scholz, The Mechanics of Earthquakes and Faulting, Cambridge Univ. Press, Cambridge, 439 pp.
[40] D.L. Wells, K.J. Coppersmith, New empirical relationship among magnitude, rupture length, rupture width, rupture area, and surface displacement, Bull. Seismol. Soc. Am. 79 (1989) 947–1002.
[41] A. Nur, E.H. Cline, Poseidon's horses: plate tectonics and earthquake storms in the late Bronze Age Aegean and Eastern Mediterranean, J. Archaeol. Sci. 27 (2000) 43–63.
[42] R. Armijo, H. Lyon-Caen, East–West extension and Holocene normal-fault scarps in the Hellenic arc, Geology 20 (1992) 491–494.
[43] J.R.M. Allen, U. Brandt, A. Brauer, H.W. Hubberten, B. Huntley, J. Keller, M. Kraml, A. Mackensen, J. Mingram, J.F.W. Negendak, N.R. Nowaczyck, H. Oberhänsli, W.A. Watts, S. Wulf, B. Zolitschka, Rapid environmental changes in southern Europe during the last glacial period, Nature 400 (1999) 740–743.
[44] O. Peyron, J. Guiot, R. Cheddadi, P. Tarasov, M. Reille, J.L. de Beaulieu, S. Bottema, V. Andrieu, Climatic reconstruction in Europe for 18,000 yr B.P. from pollen data, Quat. Res. 49 (1998) 183–196.
[45] N. D'Agostino, R. Giuliani, M. Mattone, L. Bonci, Active crustal extension in the central Apennines (Italy) inferred from GPS measurements in the interval 1994–1999, Geophys. Res. Lett. 28 (2001) 2121–2124.